Research Article

Received: 14 January 2013 Revised: 22 March 2013 Accepted: 11 April 2013 Published online in Wiley Online Library: 6 June 2013

(wileyonlinelibrary.com) DOI 10.1002/pi.4543

Morphology–performance relationship of polypropylene–nanoclay composites processed by shear controlled injection moulding

Alejandra Costantino,[a] Valeria Pettarin,[a]* Júlio Viana,[b] António Pontes,[b] António Pouzada[b] and Patricia Frontini[a]

Abstract

A nanoclay based masterbatch was mixed with polypropylene (PP) and injection moulded by conventional (CIM) and shear controlled orientation (SCORIM) injection moulding techniques. The aim was to correlate the morphologies induced by SCORIM and CIM processing with the thermal, mechanical and fracture performance of thick PP/nanoclay mouldings. In SCORIM, two extreme shear levels were applied by changing processing conditions. A complete characterization is reported, and statistical analysis was carried out to obtain a relationship between moulding properties. Nanoclay acted as a polymer morphology director, and in combination with SCORIM it induced the formation of the γ polymorph of PP. The nanoclay has a strong positive effect on the thermal degradation of PP under an oxidative atmosphere, due to the barrier effect of clay and the physico-chemical adsorption of volatile degradation products on the silicates, but there were no differences between processing techniques. SCORIM samples of neat PP showed nonlinear brittle behaviour, while nanocomposites exhibited quasi-stable behaviour induced by a large deformation capability of the skin. Although fracture initiates at practically the same loading levels, the overall propagation energy values varied with processing conditions. Statistical analysis indicates that the decrement of the core region achieved by SCORIM processing, the differences between skin and core and the PP γ phase induced by the presence of nanoclay are responsible for the toughening of SCORIM PP/nanoclay mouldings.

Keywords: polypropylene; nanoclay; non-conventional injection moulding; morphology; thermal properties; fracture behaviour

INTRODUCTION

The possibility of manufacturing polymer nanocomposites with layered silicates by melt blending techniques without the use of organic solvents and with tailored properties at low cost has gained much interest.[1–3] In the last two decades, particular interest has been paid to clay nanoplatelets (nanoclays) and their nanocomposites with non-polar thermoplastic polyolefin matrices, namely polypropylene (PP), envisaging improvement in the mechanical and permeability performance of the products.[4–6] Injection moulding trials on an industrial scale with a conventional processing setup used PP blended with nanoclay masterbatches and maleic anhydride functionalized PP as a compatibilizer.[7,8]

In principle, filling PP with a low nanoclay content (typically less than 5%) makes it adequate for engineering applications. Nevertheless, results showed only minimal improvements in stiffness and in tribological properties, while toughness was reduced particularly in weld-line regions.[9,10]

It is generally accepted that the performance of polymer nanocomposites is intimately related to the degree of dispersion of the nanofiller: good dispersion and exfoliation may lead to the expected improvement in properties.[6–11] This dispersion depends on factors such as the affinity and compatibility of the clay with the matrix, the matrix viscosity and the applied thermomechanical level, which depends on the processing conditions.[12]

PP/nanoclay composites produced by conventional injection moulding (CIM) usually display poor dispersion of the nanofillers; a combination of high back pressure and screw rotational speed improves the dispersion of the nanoclay and contributes to mechanical performance.[7,9,13] The alternative non-conventional shear control orientation in injection moulding (SCORIM) process is reported to improve the moulding properties through controlling the microstructure.[14] Significant improvements in mechanical performance, reinforcement and macromolecular alignment and elimination of internal weld lines were reported for semicrystalline polymers.[15] These result from the intense shear flow that leads

* *Correspondence to: Valeria Pettarin, Institute of Materials Science and Technology (INTEMA), University of Mar del Plata, Av. Juan B. Justo 4302, B7608FDQ Mar del Plata, Argentina. E-mail: pettarin@fi.mdp.edu.ar*

a *Institute of Materials Science and Technology (INTEMA), University of Mar del Plata, Av. Juan B. Justo 4302, B7608FDQ Mar del Plata, Argentina*

b *Institute for Polymers and Composites, IPC/I3N, Department of Polymer Engineering, University of Minho, Campus de Azurém, 4800-058 Guimarães, Portugal*

to better in-process dispersion and orientation of the fillers in the composite.[16,17] Hence, one could expect that the high shear levels applied during SCORIM would lead to a better in-process dispersion and orientation of the fillers in the moulding of nanocomposites. Promising findings concerning the use of SCORIM to manufacture PP/nanoclay composites have further encouraged us to conduct the present research.[18–21]

The present work aims to correlate the morphologies induced by CIM and SCORIM processing with the thermal, mechanical and fracture performance of PP/nanoclay mouldings. A complete characterization is therefore reported, and statistical analysis is carried out to obtain a relationship between moulding properties.

MATERIALS AND METHODS

Sample manufacturing

Compounds were based on Domolen 1100L homopolymer PP and P-802 Nanocor nanoclay masterbatch consisting of 50%PP/50%nanoclay (MB). The materials were first blended in a rotating drum at a speed of 60 rpm for 30 min. Double edge gated rectangular bars of 130 × 13 × 8 mm were injection moulded using a Ferromatik Milacron injection moulding machine type K-85A, equipped with a special mounted SCORIM mould with manifold and hydraulic system. The SCORIM process manipulates the polymer melt inside the mould cavity itself. Hydraulic pistons operating in various modes shear the melt during the holding time of the injection moulding process. These piston movements cause shearing at the solid–melt interface producing alignment of the fillers and polymer macromolecules.

A SCORIM moulding programme was defined for PP and PP with 6% MB (PP/MB-6) according to a nine-run design of experiments approach based on a three-factor and three-level orthogonal array. The processing variables considered in the moulding programme were melt temperature (200 °C, 220 °C, 240 °C); stroke time, responsible for the time of the piston movements (1 s, 2 s, 3 s); and stroke number, which is the number of piston movements (3, 7, 13). For comparison purposes CIM samples of PP and PP/MB-6 were also injected. In order to evaluate the influence of MB content, samples with 10% and 14% MB (PP/MB-10 and PP/MB-14) were injected according to run 8. This condition was selected from simulations performed using Moldex3D adopting as optimum rheological parameters the ones from our own experience.[9] Conditions and nomenclature of the injected samples are summarized in Table 1.

Sample microstructure

Samples 15 µm thick were cut with a Leitz 1401 microtome and the microstructure of the mouldings was observed with an Olympus BH2 microscope under polarized light.

DSC tests were performed on specimens that included part of the skin and part of the core structure using Perkin-Elmer equipment at a heating rate of 10 °C min^{-1}. The average global crystallinity was calculated as

$$\chi_c = \frac{\Delta H}{(1-\phi)\,\Delta H^0} \tag{1}$$

where ΔH is the apparent enthalpy of fusion per gram of composite, ΔH^0 is the heat of fusion of 100% crystalline PP, which is 207.1 kJ kg^{-1},[22] and ϕ is the MB weight fraction.

XRD analysis was performed using a Phillips X'PERT MPD diffractometer in reflection mode (Cu Kα radiation $\lambda = 1.5418$ Å, generator voltage 40 kV, current 40 mA, sample to detector distance 240 mm) to observe the PP structure in the skin and the core (Fig. 1). Measurements were recorded every 0.02° for 1 s each, varying 2θ from 2° to 40°. The interlayer distance of the nanoclay was calculated from the (001) peak using Bragg's law ($\lambda = 2d_{001}\sin\theta_{001}$). The PP α-phase orientation indices were determined as[23]

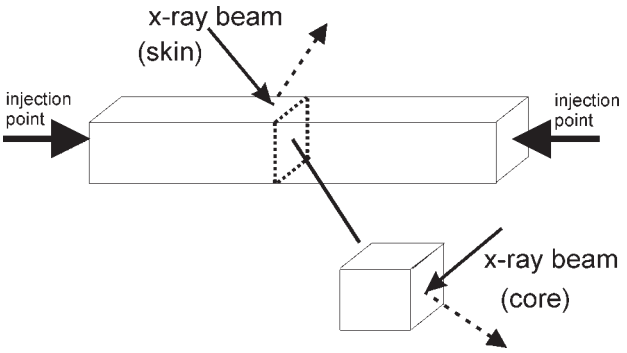

Figure 1. Setup for the XRD observations made on injection moulded bars.

$$A_{110} = \frac{I_{110}}{I_{110} + I_{111} + I_{131+041}} \tag{2}$$

$$A_{040} = \frac{I_{040}}{I_{110} + I_{040} + I_{130}} \tag{3}$$

where I_α is the peak height after background subtraction, α_1 corresponds to the (110) reflection, α_2 to the (040) reflection, α_3 to the (130) reflection and α_4 to the (111) and (041) reflections. The A_{110} index gives an indication of the orientation roughly parallel to the *c*-axis of the crystallites which in this case corresponds to the flow direction in the injected samples.[24] The A_{040} index gives an indication of a preferential molecular orientation perpendicular to the crystallite *b*-axis, i.e. more or less parallel to the sample surface.[24]

Transmission electron microscopy (TEM) microphotographs were obtained with a Jeol 100 CX microscope using an acceleration voltage of 200 kV. Samples were ultramicrotomed at room temperature with a diamond knife to a section 70 nm thick.

Overall sample performance

TGA was carried out in a Shimadzu electrobalance. Experiments were conducted at a constant rate of 10 °C min^{-1} from room temperature to 650 °C, both in nitrogen flow and in air flow. About 2 mg of material was loaded into the container. The degradation onset temperature $T_{0.1}$, at which 10% degradation occurs, the midpoint degradation temperature $T_{0.5}$ and the fraction of non-volatiles that remains at 600 °C were extracted from the mass loss in the TGA curves while the maximum decomposition temperature (T_{max}) was obtained from the derivative thermogravimetric (DTG) curves.

Viscoelastic properties were measured with a Perkin-Elmer dynamic mechanical analyzer (DMA-7) at a fixed frequency of 1 Hz in three-point bending mode, in the temperature range from −30 to 215 °C at a heating rate of 10 °C min^{-1}. The heat distortion temperature (HDT) was estimated according to ASTM D648-01 using the Scobbo method.[25]

The mechanical tests were carried out with an Instron 4467 universal testing machine at room temperature. The yield stress

Table 1. Processing conditions and nomenclature of injected samples

Processing conditions	Material			
	PP	PP/MB-6	PP/MB-10	PP/MB-14
SCORIM run 1 (st = 1 s; mt = 200 °C; sn = 3)	×	×		
SCORIM run 2 (st = 1 s; mt = 220 °C; sn = 7)	×	×		
SCORIM run 3 (st = 1 s; mt = 240 °C; sn = 13)	×	×		
SCORIM run 4 (st = 2 s; mt = 220 °C; sn = 13)	×	×		
SCORIM run 5 (st = 2 s; mt = 240 °C; sn = 3)	×	×		
SCORIM run 6 (st = 2 s; mt = 200 °C; sn = 7)	×	×		
SCORIM run 7 (st = 3 s; mt = 240 °C; sn = 7)	×	×		
SCORIM run 8 (st = 3 s; mt = 200 °C; sn = 13)	×	×	×	×
SCORIM run 9 (st = 3 s; mt = 220 °C; sn = 3)	×	×		
CIM (mt = 200 °C)	×	×		

st, stroke time; mt, melt temperature; sn, stroke number.
Constant processing setup: injection velocity 10 mm s^{-1}; injection pressure 53 bar; holding pressure 40 bar; mould temperature 30 °C; cooling time 30 s.

in compression was determined at 1 mm min^{-1} using prismatic specimens of rectangular cross-section (h = 10 mm, h/L = 1.5, h and L being the height and width of the sample) cut from the injected pieces. To avoid the eventual influence of voids developed during injection moulding, the start of the plastic domain was taken as the end of the linear part of the stress–strain plot.[26] The flexural modulus was measured according to ASTM D 790-03 at 5 mm min^{-1}. At least five samples of each kind were tested.

Fracture characterization

The fracture characterization was performed on single edge notched beam specimens (SE(B)) in three-point bending at room temperature with a constant crosshead velocity of 5 mm min^{-1} using an Instron 4467. Specimens with a span S of 52 mm and width W of 13 mm were prepared from the injected bars. Sharp notches were introduced using a Notchvis Ceast machine with a sharp fly cutter (tip radius less than 12 µm) to reach a crack-to-depth ratio a/W of 0.5. The specimens were bent until complete failure. Fracture initiation was evaluated from the critical stress intensity factor in mode I, K_{IC}, using load–line displacement plots and crack length, according to ASTM D 5045:

$$K = \frac{P}{BW^{1/2}} f(a/W) \tag{4}$$

Due to the nonlinearity of the load–displacement plots, P was determined at the intersection between a straight line with compliance 5% greater than the initial compliance and the load–displacement trace. In every case geometry validity requirements[27] were met:

$$B, a, (W - a) \geq 2.5 \left(\frac{K}{\sigma_y}\right)^2 \tag{5}$$

Besides the calculation of K_{IC}, the value of the J integral was computed from

$$J = \frac{2U}{B(W - a)} \tag{6}$$

U was calculated by integration of the load–displacement traces up to the maximum load point (J_{max} parameter determination) and up to the instability load point (J_c parameter determination).[28] J_c was computed to designate the point of unstable fracture, or loss of structural integrity, in samples displaying quasi-stable crack propagation.

Statistical analysis

To gain a better insight about the influence of each processing parameter on the final properties, the results of the experiments were evaluated by analysis of variance (ANOVA).[29]

RESULTS AND DISCUSSION

Microstructure of mouldings

Figure 2 is representative of the cross-sections of the mouldings as observed by polarized light. Consistent with expectations,[18–21] a visible difference between the shrinkage of CIM and SCORIM specimens is seen: practically no shrinkage is observed in SCORIM samples. Neat PP evidences structure development and a complete rectangular shape after use of the non-conventional moulding technique. The main difference between techniques can be observed from the photographic matching. The skin–core structure for conventionally injected specimens and the typical layered structure of the melt manipulation technique are clearly observed. The SCORIM samples feature a thick shear zone which contains many oriented layers in an onion-like microstructure. The addition of nanoclay diversified the morphology, in particular developing the shear zone into a thicker and better delineated multilayer zone.[19,30] Also an increase of the skin thickness with increase in MB content can be observed (Fig. 2).

The ANOVA of the skin layer thickness is presented in Fig. 3. The effect of the SCORIM processing variables is much higher on the PP nanocomposite than on the neat PP. For the former system, the skin layer thickness increases with stroke time and number, as would be expected as a result of a high applied shear level. Also, the skin layer thickness decreases with the melt temperature due to the high allowed relaxation time and low expected level of shear at high temperatures (lower melt viscosity).

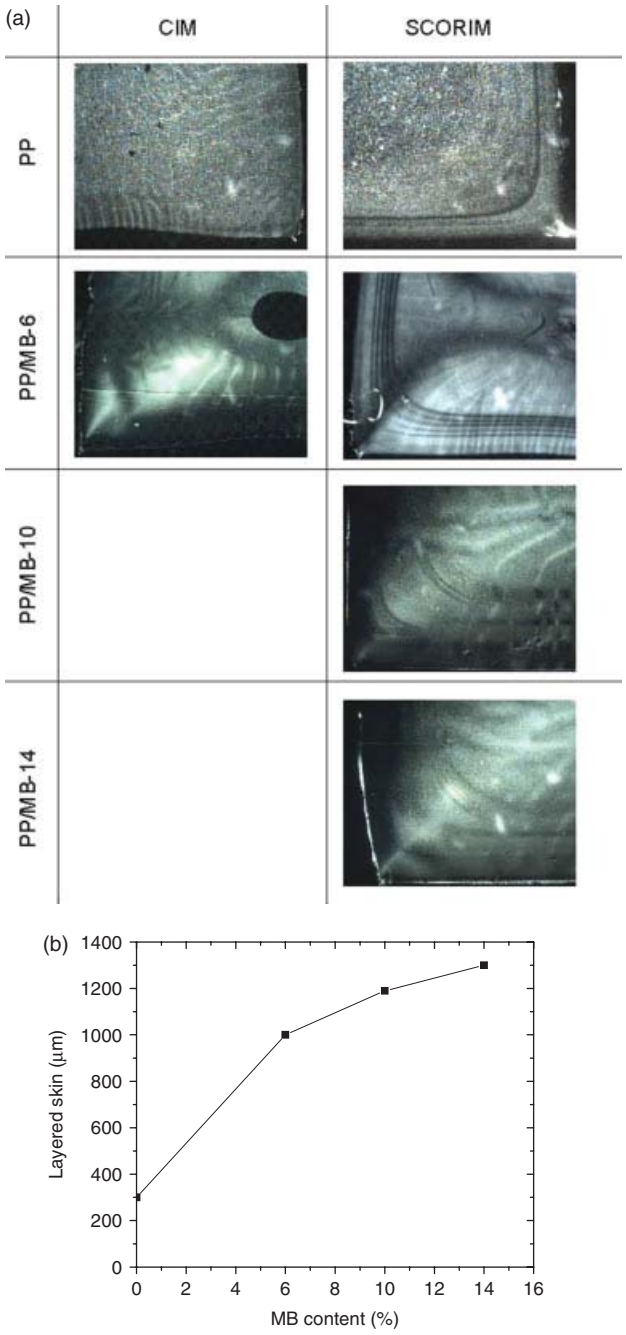

Figure 2. Polarized light results: (a) typical micrographs; (b) dependence of skin thickness on MB content.

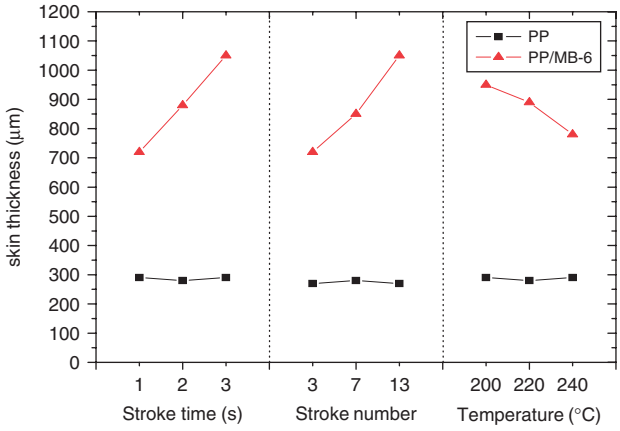

Figure 3. ANOVA of the skin thickness: effect of the processing variables.

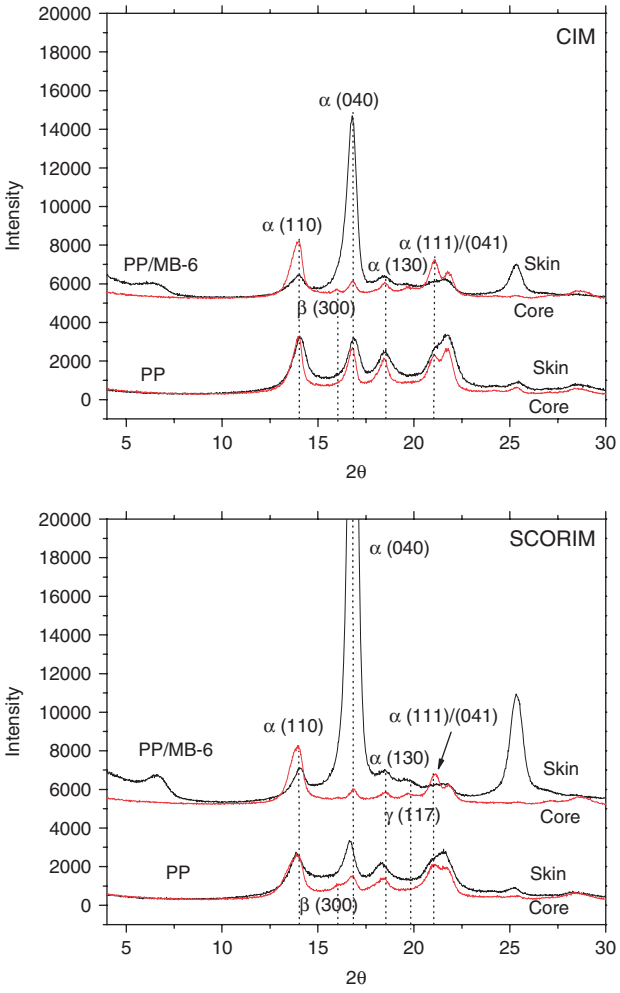

Figure 4. Typical XRD patterns of PP composites.

Morphology of the mouldings

Neat PP XRD patterns display minimal differences between CIM and SCORIM (Fig. 4). Also surface and core reflections are similar, indicating similar crystal morphology development. In the case of SCORIM, the amorphous halo is larger in the skin than in the core, anticipating a lower degree of crystallinity.

The presence of nanoclay induced significant changes in the crystal structure of PP, mainly in the skin region. Conventional injected mouldings do not exhibit β phase. SCORIM does induce some β-phase formation (the intensities of β-phase reflection from the SCORIM samples is very low in comparison with the CIM samples). The doublet (111)−(041) is smaller in X-ray patterns of SCORIM samples. This decrement indicates a higher orientation of PP molecules in SCORIM samples of PP/nanoclay,[14] since the monoclinic α phase of PP has an epitaxial relationship with the γ phase of PP such that each can grow on the lamella of the other. Marked differences in crystalline structure at the core and the surface of injected nanocomposites are observed, being more intense in the case of SCORIM pieces. Three PP polymorphs, α, β

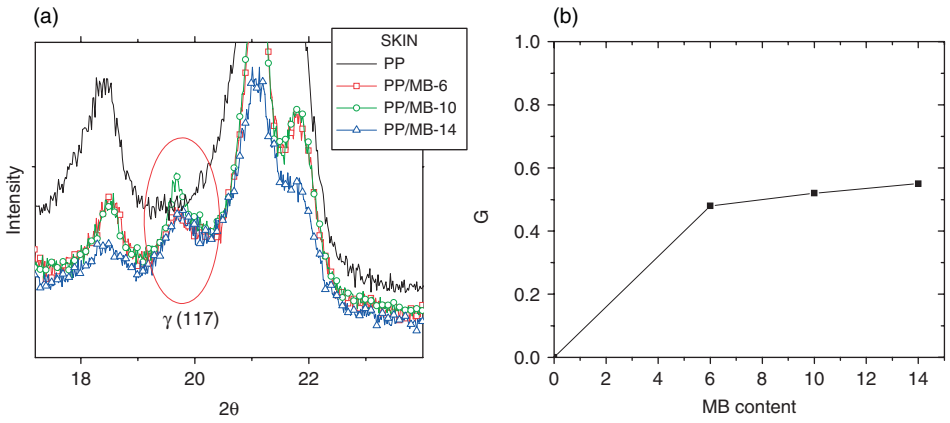

Figure 5. Evidence of the presence of γ phase in SCORIM PP/nanocomposites: (a) magnification of XRD patterns of the skin; (b) dependence of the γ-phase amount with MB content.

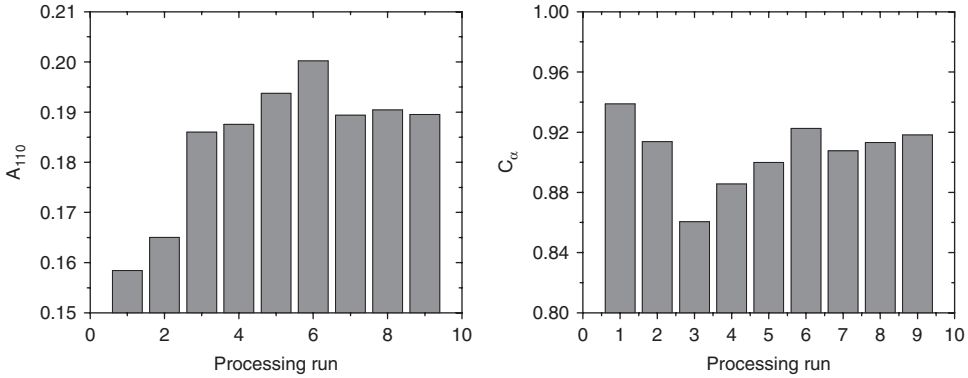

Figure 6. Crystal orientation and epitaxial index values of PP/MB-6.

and γ, were detected in the core while only α and γ polymorphs were detected in the skin. A γ-phase nucleating effect is seen in the skin of the nanocomposites (see the magnification of Fig. 5(a)). The doublet (111)−(041) is smaller in the skin than in the core, indicating a higher orientation of PP molecules in the skin layer. It seems that there are no differences in the amount or orientation of PP crystals in the core of PP/nanoclay and in neat PP. However, in the X-ray spectra of the skin of PP/nanoclay the intensities of peaks at 16.2° and 21.2° (β polymorph) were attenuated, while the intensities of peaks at 17° and 25.5° (α polymorph) and 20° (γ polymorph) were enhanced. Given that the specific diffraction peaks of α and γ phases correspond to (130)α and (117)γ, respectively, the content of crystalline γ phase (G) was evaluated using the following Turner−Jones equation:

$$G = \frac{I\gamma_{(117)}}{I\gamma_{(1117)} + I\alpha_{(130)}} \tag{7}$$

where in a generic sense $Ii(abc)$ is the intensity of the (abc) plane for each phase i.[31] It is seen that the amount of γ increases with MB content in an asymptotic way to a maximum value (Fig. 5(b)). This finding is in agreement with the results of other authors who claimed that nanoclay[32,33] and SCORIM promote the formation of γ-phase PP crystallites.[34] They proposed that the nanoclay changes the equilibrium state of the polymer (conformation) and it provides favourable sites for possible epitaxial growth of γ phase because the lattice mismatch is <10%. In summary, in these composites the nanoclay acted as α and γ nucleation sites, reducing the amount of β-form PP.

Another important feature is the marked increase of the (040)/(110) ratio for the SCORIM samples. This indicates that in SCORIM mouldings the nanoclay induced orientation of the crystalline phase of PP in the (040) direction – i.e. an increase in the degree of epitaxiality[35] – and imparted a low level of crystalline phase orientation in the flow direction. This is also revealed by the high values of the epitaxial indices C_α (Fig. 6).

Regarding the effect of the SCORIM processing conditions on morphology development, it was found that processing induces variations of A_{110} and C_α but to a small amount, especially for the latter. A_{110} and C_α seem to increase with high shearing. However, A_{110} appears to decrease for low shearing and low melt temperatures, whereas C_α decreases for low shearing and high melt temperatures. This is shown in Fig. 7, where the results from the experimental design are shown. A_{110} increases approximately 12% with stroke time, mainly for low set values, and C_α decreases with the melt temperature (about 4%).

Regarding the nanoclay, the XRD pattern of the skin layer of both CIM and SCORIM specimens shows a peak corresponding to the (001) interlayer basal spacing of the nanoclay, illustrating the intercalation of polymer between the galleries of clay layers with an intergallery space of 13.4 nm for all material systems. In contrast, the absence of this (001) peak in the core region may indicate an exfoliated structure. Other authors have previously reported similar findings for PP/clay nanocomposites.[36] They stated that the addition of nanoclay plus maleic anhydride PP (mPP) produces

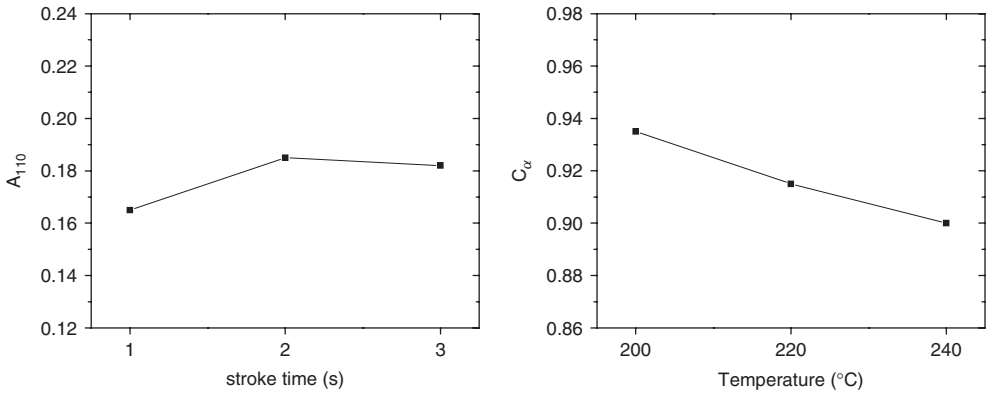

Figure 7. ANOVA of the crystal orientation and epitaxial index.

a dual effect in the PP. First, the nanoclay tends to migrate to the surface of the specimens, pulled by the maleic anhydride. This could be thought of as an effect contrary to what is desired. However, the viscosity of the system does not allow a complete and easy migration of the fillers. As a consequence of this migration effect and as the nanoclay and mPP bond to each other, the nanoclay is better exfoliated in the core, pulled by the mPP on its way to the surface. However, TEM results indicate that a marked nanoclay orientation along the flow direction in the skin layer of the injected samples is present, but complete exfoliation cannot be observed in either the skin or the core zones (Fig. 8). In fact, there are more exfoliated platelets in the skin than in the core. Regarding differences between injection techniques, higher exfoliation/intercalation of the nanoclay is seen in the SCORIM sample than in the CIM sample. This may be due to the high shear stresses exerted during SCORIM processing.

DSC results showed that the amount of overall crystallinity of PP mouldings increased with the addition of nanoclay (Fig. 9), so the nanoclay seems to act as a nucleating agent. ANOVA was also used to verify the effect of the processing variables in morphology development. A higher stroke time and number (i.e. a high shearing level) leads to a higher degree of crystallinity (Fig. 10). This may be seen as a result of the shear induced crystallization. Furthermore, the overall degree of crystallinity of the mouldings is maximized for intermediate stroke times for nanofilled and neat PP. The effect of the stroke time is different for these two material systems: when it increases the overall degree of crystallinity of the nanocomposites increases, but it decreases for neat PP. Likewise, the melt temperature has almost no effect on the overall degree of crystallinity of the nanocomposite mouldings, whilst it is maximized for intermediate values in the case of neat PP. This reflects the nucleating action of the nanoclays on PP crystallization. In general, it emerges that both high shear rate and high temperature induce a high degree of crystallinity in the PP nanocomposite.

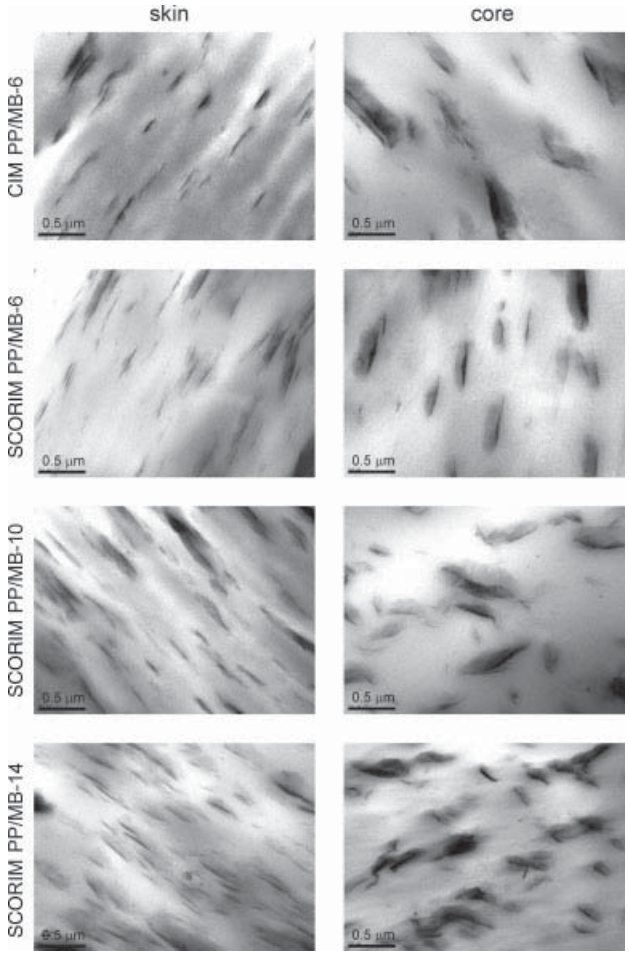

Figure 8. TEM images of the composites.

Thermal and deformation performance

A positive effect of nanoclay on the thermal degradation of PP was observed under an oxidative atmosphere, as depicted in Table 2 which shows the effect of the amount of nanoclay incorporated into the PP nanocomposite. Nanoclay presence increases the thermal stability of polymers in oxidative conditions[37] due to the nanoclay mass transport barrier effect[38] and the suppression of molecular mobility.[39] It has also been stated that the intercalated nanostructure in polymer/layered silicate nanocomposites, like that exhibited by our nanocomposites, is crucial for enhancing the thermal stability of the material.[40]

As seen in Table 2, $T_{0.1}$ increased with the addition of nanoclay (about 48 °C increment), but in the case of T_{max} and $T_{0.5}$ the increment was a steeper 87 and 94 °C, respectively. This large increment led us to infer that, besides the barrier effect, physico-chemical adsorption of volatile degradation products on the silicates occurs.[41,42]

No significant differences between CIM and SCORIM samples were found, despite slightly higher variations for the SCORIM

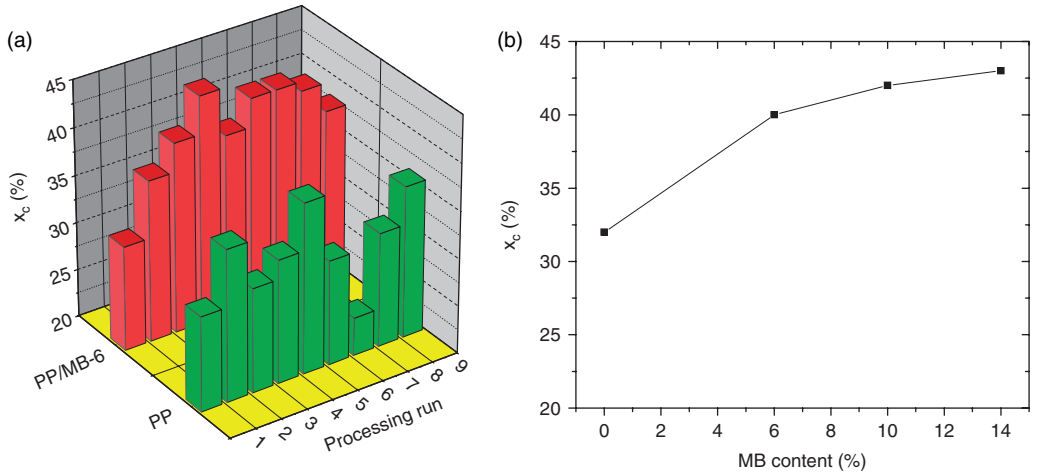

Figure 9. Degree of crystallinity of neat PP and PP/nanoclay composite samples moulded by SCORIM, as assessed by DSC: (a) effect of processing variables; (b) effect of MB content.

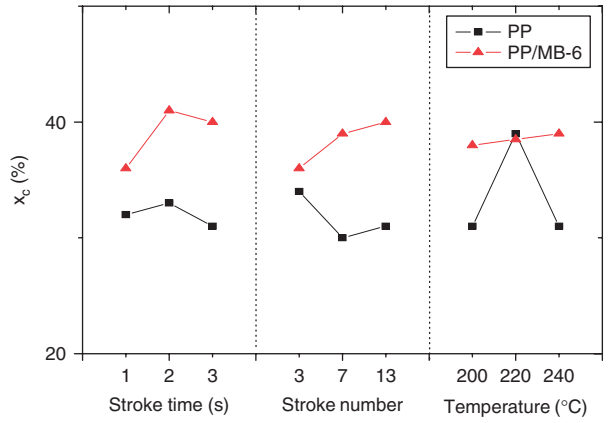

Figure 10. ANOVA of the degree of crystallinity: effect of the processing variables.

samples. This indicates that the thermal stability of the composites is not dependent on the PP microstructure developed by SCORIM processing but rather on the clay content.

As shown in Table 3, the incorporation of nanoclay increases the HDT slightly: by 10 °C in CIM and 4 °C in SCORIM. Usually the addition of nanoclay into the PP matrix causes an increase in the HDT of the mouldings by about 5 and 10 °C.[43,44] Moreover, the morphology developed during SCORIM increased HDT by *ca* 20 °C for both PP and PP/nanoclay mouldings, indicating that HDT is highly dependent on the microstructure induced by the melt manipulation in SCORIM.

Table 3. Results obtained from HDT measurements

HDT (°C)	CIM	SCORIM
PP	45	68
PP/MB-6	55	72

Figure 11 presents the flexural modulus and compressive yield stress as a function of the percentage of nanoclay incorporated. The yield stress of the nanocomposites was slightly larger than that of neat PP, but was almost unchanged with nanoclay content. Trends reported in the literature are contradictory, reporting either an increase or decrease in properties with addition of nanoclay.[45] A quite significant increase in flexural modulus of the nanocomposites in comparison with neat PP was also found, of the order of 40%. From theoretical predictions using the Mori–Tanaka composite micromechanical model, Bayar *et al.* estimate the increase in the elastic modulus of PP with 3%–6% of nanoclay to be of the same order.[46] For a low percentage of nanoclay incorporated, in the range 1%–6%, the variations in the elastic modulus are negligible, increasing thereafter. Besides the amount of nanoclays, intercalated morphologies may also restrict the mobility of polymer chains contributing to improvement of the modulus.[47,48] Furthermore, in flexural tests, the mechanical response is governed by the most exterior fibre, i.e. the skin of injected samples. In these samples, the PP microstructure of the skin layer changed with the addition of nanoclay, but the microstructural features are independent of the nanoclay content. Due to the segregation effect of clay into the skin, it seems that

Table 2. Results obtained from TGA and DTG curves

	Material	$T_{0.1}$ (°C)	$T_{0.5}$ (°C)	T_{max} (°C)	Char (%)
SCORIM	PP	296	337	342	2.5
	PP/MB-6	319	400	426	3.4
	PP/MB-10	336	418	446	5.6
	PP/MB-14	342	424	436	6.2
CIM	PP	294	340	354	1.8
	PP/MB-6	311	398	422	3.2

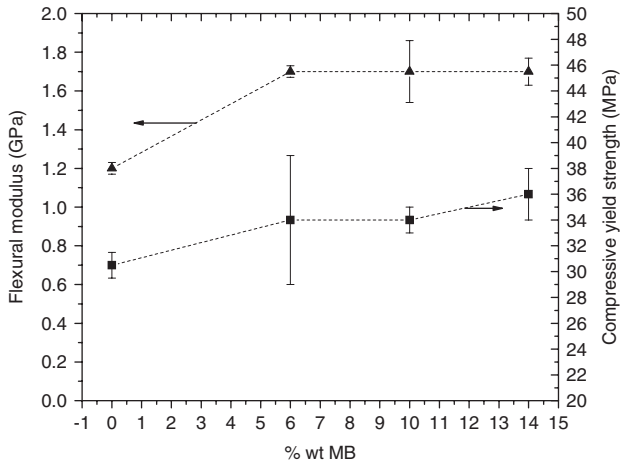

Figure 11. Mechanical properties of PP/nanoclay composites.

the effective content of clay in the skin is similar irrespective of MB concentration, and hence the modulus.

Fracture performance

Several micro-mechanisms have been proposed as probably responsible for the toughness enhancement of polymer nanocomposites. The occurrence of each mainly depends on the orientation of the nanoclay to the loading direction and on the degree of nanoclay dispersion and disagglomeration. Some mechanisms are associated with the nanoclay, such as splitting of stacked nanoclay particles if they are oriented perpendicular to the loading direction; opening at a certain angle for tilted nanoclay agglomerates; sliding of stacked particles if they are parallel to the deformation;[49,50] and delamination of nanoclay particles.[51] Other mechanisms are intrinsically associated with the semicrystalline nature of the matrix, such as the initiation of multiple crazes at the pole of delaminated nanoclay particles. Besides, the formation of small needle-like voids which provoke whitening of the specimen may occur. Massive fibrillation due to the generation of voids at the particle–matrix interface and subsequent growth and coalescence developing a sheet-like structure has also been reported.[52–54] Moreover distinct differences in the deformation behaviour in the skin and core have been reported for nanocomposite injection mouldings.[9] All these mechanisms dissipate different amounts of energy. Samples exhibited different fracture stabilities ranging from a modest nonlinearity to a quasi-stable regime. The fracture regime was found to be dependent upon the material type and the injection moulding conditions.

In this work, PP shows nonlinear behaviour and unstable brittle fracture after reaching maximum load. Load–displacement curves dropped to zero instantaneously upon reaching the maximum

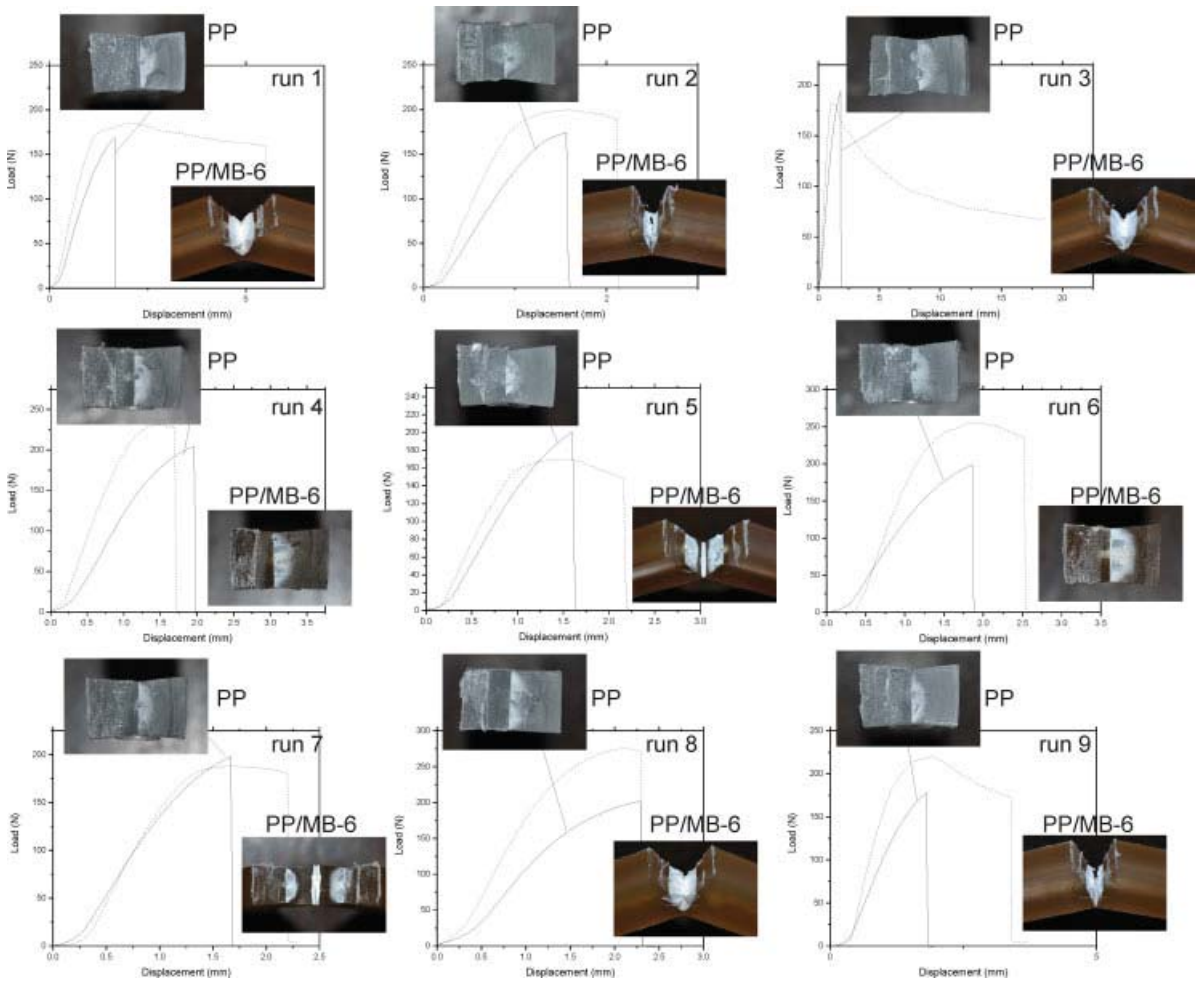

Figure 12. Fracture load *versus* displacement curves for SCORIM samples including fracture surfaces.

Table 4. Fracture parameters for different experimental runs

Run	K_{IC} (MPa m$^{1/2}$)		J_{max} (N mm^{-1})		J_c (N mm^{-1})			
					All samples		Samples with no visible defects	
	PP	PP/MB-6	PP	PP/MB-6	PP	PP/MB-6	PP	PP/MB-6
1	1.4 ± 0.2	1.6 ± 0.3	6.7 ± 1	10.25 ± 3.7	6.7 ± 1	58.2 ± 35.9	6.7 ± 1	94.5 ± 7.8
2	1.45 ± 0.3	1.5 ± 0.3	6 ± 1	7 ± 0.8	6 ± 1	20 ± 13.7	6 ± 1	[a]
3	1.25 ± 0.1	1.3 ± 0.2	7 ± 1	5 ± 2	7 ± 1	54 ± 25.8	7 ± 1	65.5 ± 3
4	1.5 ± 0.3	1.6 ± 0.1	11 ± 8.7	7.75 ± 1	11 ± 8.7	10.8 ± 3.5	7.2 ± 0.9	8.3 ± 1.2
5	1.3 ± 0.2	1.4 ± 0.3	7.2 ± 1.6	5 ± 1.2	7.2 ± 1.6	14.8 ± 8	6.5 ± 0.6	23.5 ± 2.1
6	1.3 ± 0.1	1.7 ± 0.2	8.4 ± 1.9	7.5 ± 2	8.4 ± 1.9	10.4 ± 3.3	8.4 ± 1.9	10.4 ± 3.2
7	1.3 ± 0.2	1.6 ± 0.1	8.8 ± 3.8	7.3 ± 1.5	8.8 ± 3.8	11.3 ± 4.7	7 ± 0.01	9 ± 1.7
8	1.6 ± 0.4	1.8 ± 0.1	8.4 ± 2.1	11 ± 2.5	8.4 ± 2.1	40.4 ± 35.4	8.4 ± 2.1	78.5 ± 13
9	1.2 ± 0.1	1.4 ± 0.3	6 ± 1.2	6.5 ± 2	6 ± 1.2	16.4 ± 11.9	6 ± 1.2	[a]

[a] Neglected behaviour.

load at relatively short displacement levels (Fig. 12). Acceptable results were found for SCORIM samples but not for CIM: while only a few SCORIM conditions resulted in samples with notable voids and defects, there were voids in the majority of CIM mouldings. With regard to PP mouldings, there were no significant differences in K_{IC} and J values with varying processing conditions (Table 4).

The PP/nanoclay mouldings produced by CIM showed large voids generated during processing. These samples show an apparently stable fracture with crack arrest regime induced by the presence of large voids, which partially relaxed the triaxiality, and different maximum load values were reached in every case (see the examples shown in Fig. 13). These samples were discarded in the results analysis. In contrast, composites produced by SCORIM led to acceptable mouldings and only few samples displayed visible defects. They showed different load–displacement patterns. Most of them exhibited quasi-stable behaviour. The load increased nonlinearly, and then it was maintained up to a certain displacement level when a drastic drop occurred (Fig. 12). Moreover, in many samples (processing conditions 1, 2, 3, 5, 8 and 9) a large deformation of the skin was observed (Fig. 12). It should be mentioned here that this skin effect characterized by tail instability in load–displacement curves has been found previously for PP based systems.[55] This large deformation of the skin layer can be related to the high level of molecular and nanoclay orientation (Fig. 8) which favours the sliding of the macromolecules (fostered by the oriented nanoclays), thus improving the deformation capability. In fact, it has been pointed out that the development of necking is probably a combined effect of skin–core ratio, skin orientation and possible morphology rearrangement in the skin under different loading directions influenced also by heat evolution and dissipation processes. Since SCORIM induces a thicker multi-layered skin in the PP/nanoclay mouldings, the skin effect is favoured. This phenomenon leads to differences in the load–line displacement curves promoting a more stable crack propagation followed by a necking phase of highly different extension (skin effect).[9,56] If voids appeared in the fracture surface, they inhibited the skin effect.

In the results obtained for these PP/nanoclay composites, small differences were displayed by K_{IC} and J_{max} (which are related to fracture initiation), but large differences in J_c (which is related to fracture propagation) were found (Table 4). Replicas of each condition show a significant scatter provoked by a combination of different causes. The differences obtained for each condition

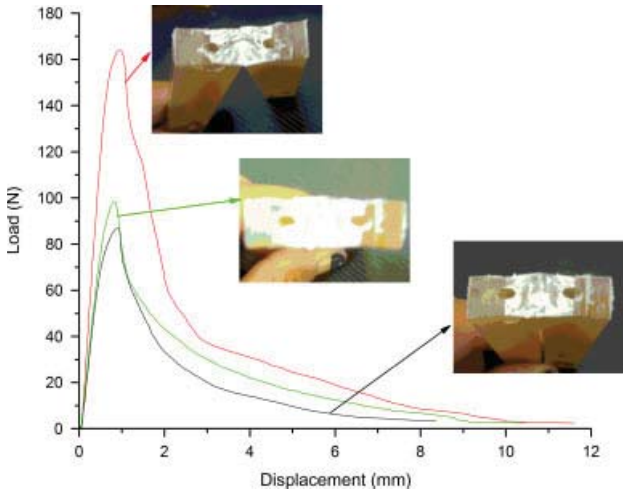

Figure 13. Load *versus* displacement curves for PP/nanoclay mouldings which presented large voids generated during CIM.

are typical of semicrystalline polymer injected parts influenced by microstructural parameters, which include crystalline structure, degree of crystallinity, supermolecular structure or skin–core configuration.[57] In addition, this kind of material is considered to be in the ductile to brittle transition regime which implies large scatter[58] due to dissimilar contributions of plastic flow and stable crack growth in different specimens of the same set. In fact, when J values were assessed as J_c taking into account all samples, the scatter is actually inadmissible in some conditions. However, if values are calculated discarding samples with visible defects, scatter diminished considerably and values became acceptable (see Table 4).

The addition of clay improved the fracture performance of PP SCORIM samples thanks to the differences induced by nanoclay in the microstructure described above: it refines the crystal structure and promotes epitaxial growth of the γ phase. This γ phase induces a large-scale plastic deformation with consequent tearing of matrix ligaments leading to fibrillation, responsible for higher toughness in relation to neat PP.[59] The best global results (skin effect with high J value and good reproducibility) were achieved in run 1 which implies low temperature and shear level.

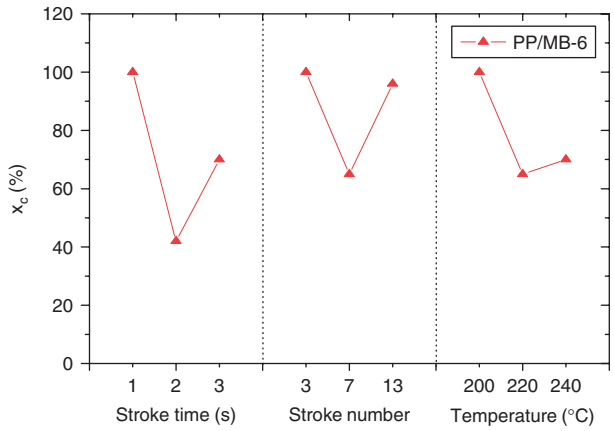

Figure 14. ANOVA of J_c values: effect of the processing variables.

Table 5. Influence of shear and thermal levels upon the morphology development and and mechanical properties of SCORIM mouldings for 3% nanoclay incorporation in PP nanocomposites

Property	Shear level increment	Thermal level increment
Morphology		
Skin thickness	▲▲	▼
Skin crystallinity	▲	▼▼
Overall crystallinity	▲	▲
Skin orientation	▲	–
Skin epitaxiality degree	▲	▲▲
Mechanical		
J_c	▼	▼

The ANOVA in Fig. 14 indicates that an increment in the shear level (higher stroke number and time) leads to a decrease in J_c value. As mentioned, an increase in the crystalline phase orientation and the skin crystallinity and thickness was found with increasing shear level. Also, ANOVA shows that J_c decreases with increment in melt temperature (Fig. 14). This is in concordance with the increase in orientation (A_{110}) and decrease in skin crystallinity and thickness. Table 5 shows the influence of the shear and thermal level applied in SCORIM on the morphology development and J_c values of PP/MB-6 composite. The analysis of these results seems to indicate that the most relevant morphology feature is the skin orientation and crystallinity in the flow direction: higher skin orientation levels and crystallinity induce a lower toughness (see Fig. 15).

CONCLUSIONS

In this work, PP/nanoclay composites produced by SCORIM were characterized. It was found that the incorporation of nanoclay changes the developed morphology upon processing. Adding nanoclay to PP results in a low level of crystalline phase orientation in the flow direction and increment in the degree of epitaxiality. Nanoclays also act as α- and γ-phase nucleating agents, diminishing the β phase and increasing the degree of epitaxiality. Macroscopically, the PP SCORIM samples exhibit a well defined shear-core structure: a centre core which occupies less than typical CIM moulded parts and a shear zone reinforcing the structure. In nanocomposites, a multilayer structure occupies

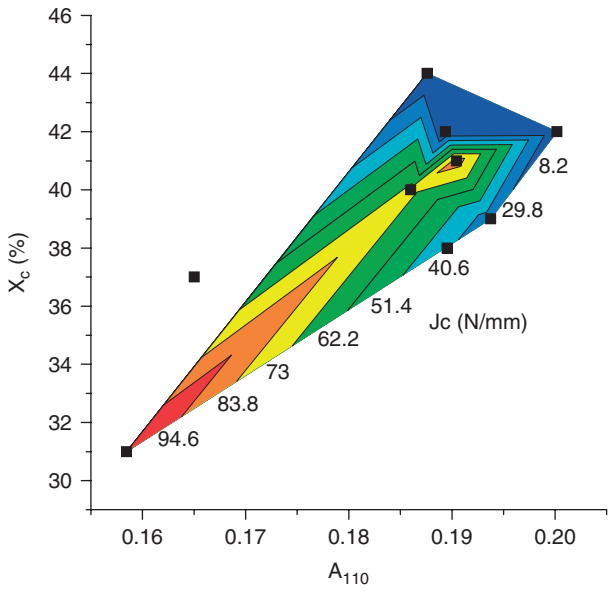

Figure 15. Correlation between J_c values and morphology parameters.

more than twice the thickness of the shear zone of PP pieces, i.e. there is even less core.

The nanoclay has a strong positive effect on the thermal degradation of PP in an oxidative atmosphere. However, no significant differences between CIM and SCORIM samples were found, indicating that thermal stability of the composites is not dependent on the PP structure developed by SCORIM processing. On the other hand, the addition of nanoclay and melt manipulation during SCORIM have a synergistic effect increasing the PP HDT.

SCORIM samples of neat PP showed nonlinear brittle behaviour, while nanocomposites exhibited quasi-stable behaviour induced by a large deformation capability of the skin. Although fracture initiates at practically the same loading levels, the overall propagation energy values varied with processing conditions.

Statistical analysis indicates that the decrement of the core region achieved by SCORIM processing, the differences between skin (or shear zone) and core and the PP γ phase induced by the presence of nanoclay are responsible for the toughening of SCORIM PP/nanoclay thick mouldings.

ACKNOWLEDGEMENTS

The authors thank the National Research Council of Argentina (CONICET), the MINCyT (Argentina) and the FCT – Fundação para a Ciência e Tecnologia (Portugal) for financial support of this research.

REFERENCES

1 Sinha Ray S and Okamoto M, *Prog Polym Sci* **28**: 1539–1641 (2003).
2 Vaia RA, Ishu H and Giannelis EP, *Chem Mater* **5**: 1694–1696 (1993).
3 Frontini P and Pouzada A, *Express Polym Lett* **5**: 661–661 (2011).
4 Alexandre M and Philippe D, *Mater Sci Eng* **28**: 1–63 (2000).
5 Manias W, Touny A, Wu L, Strawhecker K, Lu B and Chung TC, *Chem Mater* **13**: 3516–3523 (2001).
6 Paul DR and Robeson LM, *Polymer* **49**: 3187–3204 (2008).
7 Rajesh JJ, Soulestin J, Lacrampe MF and Krawczak P, *Express Polym Lett* **6**: 237–248 (2012).
8 Frache A, Monticelli O, Ceccia S, Brucellaria A and Casale A, *Polym Eng Sci* **48**: 2373–2381 (2008).
9 Pettarin V, Brun F, Viana J, Pouzada A and Frontini P, *Compos Sci Technol* **74**: 28–36 (2013).

10 Troughton MJ, *Handbook of Plastics Joining*, 2nd edn, William Andrew Publishing, Boston, MA, Chapter 35: Polypropylene pp. 395–417 (2009).
11 Bousmina M, *Macromolecules* **39**: 4259–4263 (2006).
12 Dennis HR, Hunter DL, Chang D, Kim S, White JL, Cho JW *et al.*, *Polymer* **42**: 9513–22 (2001).
13 Pettarin V, Viau G, Fasce L, Viana J, Pontes A, Frontini P *et al.*, *Polym Eng Sci* (2013).
14 Kalay G and Bevis MJ, *J Polym Sci Pol Phys* **35**: 265–291 (1997).
15 Kikuchi A, Coulter JP and Angstadt DC, *J Injection Molding Technol* **6**: 91 (2002).
16 Tang H, Chen J-B, Wang Y, Xu J-Z, Hsiao BS, Zhong G-J *et al.*, *Biomacromolecules* **13**: 3858–3867 (2012).
17 Costantino A, Pettarin V, Viana J, Pontes A, Pouzada A and Frontini P, *Procedia Mater Sci* **1**: 34–43 (2012).
18 Bilewicz M, Viana JC, Cunha AM and Dobrzanski LA, *J Achievements Mater Manufacturing Engineer* **15**: 159–165 (2006).
19 Bilewicz M, Viana JC and Dobrzanski LA, *J Achievements Mater Manufacturing Engineer* **24**: 43–46 (2007).
20 Bilewicz M, Viana JC and Dobrzanski LA, *J Achievements Mater Manufacturing Engineer* **31**: 71–76 (2008).
21 Bilewicz M, Viana JC and Dobrzanski LA, *Arch Mater Sci Engineer* **30**: 69–72 (2008).
22 Brandrup J, Immergut EH, Grulke EA, Abe A and Bloch DR, *Polymer Handbook*. Wiley, New York (1999).
23 Trotignon JP, Lebrun JL and Verdu J, *Plast Rub Proc Appl* **2**: 247–251 (1982).
24 Zhu PW and Edward G, *Macromol Mater Eng* **288**: 301–311 (2003).
25 Scobbo JJ, Thermomechanical performance of polymer blends, in *Polymer Blends*, vol. 2, ed. by Paul DR and Bucknall CB. Wiley, New York, pp. 335–357 (2000).
26 Cauvin L, Kondo D, Brieu M and Bhatnagar N, *Polym Test* **29**: 245–250 (2010).
27 Williams JG and Cawood MJ, *Polym Test* **9**: 15–26 (1990).
28 Fasce L, Frontini P, Wong SC and Mai YW, *J Polym Sci Pol Phys* **42**: 1075–1089 (2004).
29 Henderson J, Ball AK and Zhang JZ, Cycle time reduction for optimization of injection moulding machine parameters for process improvement, in *Proceedings of the 2006 IJME – Intertech International Conference on Engineering & Technology, October 19–21, 2006 - Kean University, Kentucky, USA*, ENT 105-039.
30 Dobrzanski LA, Krol M, Bilewicz M and Viana JC, *J Achievements Mater Manufacturing Engineer* **27**: 19–22 (2008).
31 Turner-Jones A, *Polymer* **12**: 487 (1971).
32 Yuan Q, Deshmanca C, Pesacreta TC and Misra RDK, *Mater Sci Eng Struct* **480**: 181–188 (2008).
33 Yuan Q, Chen J, Yang Y and Misra RDK, *Mater Sci Eng Struct* **527**: 6002–6011 (2010).
34 Kalay G, Zhong Z, Allan P and Bevis MJ, *Polymer* **37**: 2077–2085 (1996).
35 Kim B, Lee SH, Lee D, Ha B, Park J and Char K, *Ind Eng Chem Res* **43**: 6082–6089 (2004).
36 Hernandez-Luna A, Structure property and deformation analysis of polypropylene montmorillonite nanocomposites. PhD Thesis, University of North Texas (2003).
37 Tidjani A, Wald O, Pohl MM, Hentschel MP and Schartel B, *Polym Degrad Stabil* **82**: 133–140 (2003).
38 Qui L, Chen W and Qu B, *Polymer* **47**: 922–930 (2006).
39 Leszczyńskaa A, Njugunab J, Pielichowskia K and Banerjeec JR, *Thermochimica Acta* **453**: 75–96 (2007).
40 Lee D and Char K, *Polym Degrad Stab* **75**: 555–560 (2002).
41 Zanetti M, Camino G, Reichert P and Mülhaupt R, *Macromol Rapid Commun* **22**: 176–180 (2001).
42 Qin H, Zhang S, Zhao C, Feng M, Yang M, Shub Z *et al.*, *Polym Degradation Stability* **85**: 807–813 (2004).
43 Martins CG, Larocca NM, Paul DR and Pessan LA, *Polymer* **50**: 1743–1754 (2009).
44 Santos KS, Liberman SA, Oviedo MAS and Mauler RS, *Composites A* **40**: 1199–1209 (2009).
45 Szazdi L, Pukanszky Jr B, Vaneso GJ and Pukanszky B, *Polymer* **47**: 4638–4648 (2006).
46 Bayar S, Delate F, Li J, Effect of temperature on mechanical properties of nanoclay reinforced polymeric nanocomposites - part ii: modeling and theoretical predictions, *Journal of Composite Materials*, in press.
47 Pinnavaia TJ and Beall GW, *Polymer—Clay Nanocomposites*. John Wiley, New York (2000).
48 Gloaguen JM and Lefebvre JM, *Polymer* **42**: 5841–5847 (2001).
49 Kim GM, Lee DH, Hoffmann B, Kressler J and Stöppelmann G, *Polymer* **42**: 1095–1100 (2001).
50 Kim GM, Goerlitz S and Michler GH, *J Appl Polym Sci* **105**: 38–48 (2007).
51 Cotterell B, Chia JYH and Hbaieb K, *Eng Fract Mech* **74**: 1054–1078 (2007).
52 Bureau MN, Perrin-Sarazin F and Ton-That MT, *Polym Eng Sci* **44**: 1142–1151 (2004).
53 Bureau MN, Ton-That MT and Perrin-Sarazin F, *Eng Fract Mech* **73**: 2360–2374 (2006).
54 Saminathan K, Selvakumar P and Bhatnagar N, *Polym Test* **27**: 453–458 (2008).
55 Karger-Kocsis J and Mouzakis DE, *Polym Eng Sci* **39**: 1365–1374 (1999).
56 Heino M, Hietaoja P, Seppälä J, Harmia T and Friedrich K, *J Appl Polym Sci* **66**: 2209–2220 (1997).
57 Aurrekoetxea J, Sarrionandia MA, Urrutibeascoa I and Maspoch ML, *Polymer* **44**: 6959–6964 (2003).
58 Cocco RG, Frontini PM and Perez Ipiña JE, *J Polym Sci Polym Phys* **43**: 3674–3684 (2005).
59 Yuan Q, Deshmane C, Pesacreta TC and Misra RDK, *Mater Sci Eng A* **480**: 181–188 (2008).

